Gu, YuanTong and Yarlagadda, Prasad K. (2009) A bridging transition technique for the combination of meshfree method with finite element method in 2D solids and structures. Computational Mechanics, 44. pp. 119-131.

Comput Mech (2009) 44:119–131
DOI 10.1007/s00466-008-0359-y

A bridging transition technique for the combination of meshfree method with finite element method in 2D solids and structures

Y. T. Gu* and Prasad K.D.V. Yarlagadda

School of Engineering Systems,
Queensland University of Technology
2 George St, GPO Box 2434, Brisbane QLD 4001, Australia

Abstract

For certain continuum problems, it is desirable and beneficial to combine two different methods together in order to exploit their advantages while evading their disadvantages. In this paper, a bridging transition algorithm is developed for the combination of the meshfree method (MM) with the finite element method (FEM). In this coupled method, the meshfree method is used in the sub-domain where the MM is required to obtain high accuracy, and the finite element method is employed in other sub-domains where FEM is required to improve the computational efficiency. The MM domain and the FEM domain are connected by a transition (bridging) region. A modified variational formulation and the Lagrange multiplier method are used to ensure the compatibility of displacements and their gradients. To improve the computational efficiency and reduce the meshing cost in the transition region, regularly distributed transition particles, which are independent of either the meshfree nodes or the FE nodes, can be inserted into the transition region. The newly developed coupled method is applied to the stress analysis of 2D solids and structures in order to investigate its' performance and study parameters. Numerical results show that the present coupled method is convergent, accurate and stable. The coupled method has a promising potential for practical applications, because it can take advantages of both the meshfree method and FEM when overcome their shortcomings.

KEYWORDS: Numerical Analysis; Coupled Method; Meshfree Method; Finite Element Method; Bridging transition;

* E-mail: yuantong.gu@qut.edu.au

Comput Mech (2009) 44:119–131
DOI 10.1007/s00466-008-0359-y

1 Introduction

Numerical techniques have been developed and used to solve partial differential equations (PDEs) for long time. From the last century, the finite element method (FEM) has become a dominated numerical modelling and simulation tool for the analysis of solids and structures. FEM commercial software packages are widely used in academic research and industries. Moreover, because of the rapid development of engineering and science, some practical problems (e.g., the metal forming problem and dynamic fracture problem) become even more challenging. The shortcomings of FEM have been revealed because of the use of the pre-defined meshes and elements. For example, FEM often has poor accuracy, especially for stress fields, and it often has difficulty in adaptive analysis. To overcome these shortcomings, the concept of meshfree (meshless) method (MM) has been proposed. Many meshfree methods have been developed so far including: the smooth particle hydrodynamics (SPH) (Gingold and Moraghan, 1977), the element-free Galerkin (EFG) method (Belytschko et al., 1994), the meshfree finite difference method (Krok and Orkisz, 1989; Liszka and Orkisz, 1977), the reproducing kernel particle method (RKPM) (Liu et al., 1995; Liew et al. 2002), the meshfree local Petrov-Galerkin (MLPG) method (Atluri and Zhu, 1998; Atluri and Shen, 2002; Gu and Liu, 2001a), the local radial point interpolation method (LRPIM) (Gu and Liu, 2001b; Liu and Gu, 2001; Wang et al., 2003; Zhang et al., 2007), and so on.

It has been reported that the meshfree method has many advantages including: a) good accuracy for stress field, 2) effectiveness for adaptive analysis, and 3) applicability for some special problems. However, many meshfree techniques have worse computational efficiency than FEM, because more computational cost is required in the meshfree interpolation and numerical integrations (Liu and Gu, 2005). To improve the computational efficiency, some strategies have been developed. For example, a group of meshfree approaches (or called the modified FEM), which try to attain FEM efficiency directly, have been developed. The generalized FEM (GFEM) (Duarte and Kim, 2007; Strouboulis et al. 2000) is one instance of the partition of unity method. Several meshfree methods proposed in recent years can be viewed as GFEM including finite element partition of unity method (Babuska and Melenk, 1997; Griebel and Schweitzer, 2000; Melenk and Babuska,1996; Schweitzer, 2003), *hp* clouds (Duarte, 1996), the eXtended FEM (X-FEM)(Chessa et al., 2002), etc. However,, how to improve the computational efficiency of the meshfree method is still an open problem (Liu and Gu, 2005).

Comput Mech (2009) 44:119–131
DOI 10.1007/s00466-008-0359-y

For certain problems, for example a small crack in a big base or a structure standing on a big foundation, it is desirable and beneficial to combine a few existing numerical methods together in order to exploit their advantages while evade their disadvantages. This idea has been successfully used in the combination of FEM and the boundary element method (BEM) (Brebbia et al., 1984). The similar idea has also been employed to develop the coupled meshfree methods with other existing numerical methods. Belytschko and Organ (1995) firstly coupled EFG with FEM through interface FEM elements and the modified meshfree interface shape functions. Hegen (1996) developed another coupled EFG/FEM technique based on the modified variational principle. Gu and Liu developed a group of coupled methods including EFG/BEM and MLPG/FEM/BEM (Gu and Liu, 2001c, 2003, 2005; Liu and Gu, 2000a,b) based on the FE interface element technique or the modified variational principle. In these coupled methods, the meshfree method (MM) is used in a sub-domain where the MM is required to obtain high accuracy, and FEM or BEM is employed in other sub-domains where FEM or BEM is required to improve the computational efficiency.

The major difficulty in the development of the combination of the meshfree method and FEM or BEM is how to satisfy the high-order compatibility conditions on the interface between different domains of these two different methods. Summarily, two combination techniques have been proposed to enforce the compatibility conditions: 1) the method using the FE interface element (Belytschko and Organ, 1995; Gu and Liu, 2001c), and 2) the method using modified weak forms (Hegen,1996; Gu and Liu, 2003). However, there are still some technical issues to ensure the compatibility in these two techniques. In these two techniques, two different domains of the FEM domain, $\Omega_{(FE)}$, and the meshfree domain, $\Omega_{(MM)}$ are connected through a common boundary (i.e., a interface curve for a 2D problem and a interface surface for a 3D problem), called the interface. In addition, it is difficult to ensure the high-order compatibility only through a curve or surface interface boundary. Along this interface boundary, the meshfree nodes and the FEM nodes coincide with each other, and are dependent on each other. It makes the mesh- and node-generation are difficult, especially in sub-domains along the interface. These two techniques and their shortcoming have been summarized by Gu and Liu (2005).

Recent years, in the development of nanotechnology, the so-called multiscale (crossing macro-, micro- and nano- scales) modeling and simulation are becoming important for micro/nano-mechanics. The coupled continuum FEM/molecular dynamic (MD) methods have been proposed and applied to the multiscale analysis (Abraham et al., 1998). A bridging algorithm has been developed (Wagner and Liu, 2003; Xiao and Belytschko, 2004; Gu and

Comput Mech (2009) 44:119–131
DOI 10.1007/s00466-008-0359-y

Zhang, 2006) for multiscale simulation for micro/nano-mechanics. In this multiscale technique, a bridging region is applied to cross the different scales, which are solved by continuum and atomic numerical techniques, respectively. The energy can be smoothly transferred through this bridging region, and the motion (displacement and velocity) compatibility can be also ensured. Based on the idea of the bridging algorithm for micro/nano multiscale analysis, a continuum bridging transition technique is proposed in this paper to develop an advanced coupled meshfree method (MM)/FEM technique.

In the coupled MM/FEM simulation, the problem domain is divided into several sub-domains: one sub-domain is simulated by the meshfree method, and the other sub-domains are simulated by FEM. These two parts are connected by a transition (bridging) region. A bridging transition technique using the modified variational principle and the transition particles is proposed to ensure a seamless transition between MM and FEM sub-domains. Numerical studies are presented to demonstrate the effectiveness of the newly developed coupled method. Some important parameters which affect the performance of the coupled method are also thoroughly studied. The outline of this paper is as follows: Section 2 briefs the formulations of the meshfree method and FEM. Section 3 discusses the combination condition and presents the new bridging transition algorithm. The detailed formulation of the advanced coupled MM/FEM method is also presented in this section. Section 4 gives the numerical studies, and a remark is presented in Section 5.

2 Discrete equations of the meshfree method and FEM

Consider the following two-dimensional (2D) problem of solid mechanics (Liu and Gu, 2005) in a domain Ω bounded by Γ:

$$\nabla\boldsymbol{\sigma}+\mathbf{b}=0 \qquad \text{in } \Omega \tag{1}$$

where $\boldsymbol{\sigma}$ is the stress tensor, which corresponds to the displacement field $\mathbf{u}=\{u, v\}^{\mathrm{T}}$, $\mathbf{b}$ is the body force vector, and ∇ is the divergence operator. The boundary conditions are given as follows:

$$\mathbf{u} = \bar{\mathbf{u}} \qquad \text{on } \Gamma_{\mathrm{u}} \tag{2}$$

$$\sigma \cdot \mathbf{n} = \bar{\mathbf{t}} \qquad \text{on } \Gamma_{\mathrm{t}} \tag{3}$$

in which the superposed bar denotes prescribed boundary values and $\mathbf{n}$ is the unit outward normal to domain Ω.

The total potential energy Π can be given by

Comput Mech (2009) 44:119–131
DOI 10.1007/s00466-008-0359-y

$$\Pi = \int_{\Omega} \frac{1}{2} \boldsymbol{\varepsilon}^{\mathrm{T}} \cdot \boldsymbol{\sigma} \, \mathrm{d}\Omega - \int_{\Omega} \mathbf{u}^{\mathrm{T}} \cdot \mathbf{b} \mathrm{d}\Omega - \int_{\Gamma_t} \mathbf{u}^{\mathrm{T}} \cdot \bar{\mathbf{t}} \mathrm{d}\Gamma \tag{4}$$

with the boundary condition, Equation (2), where $\boldsymbol{\varepsilon}$ is the strain.

The meshfree method and FEM use the similar global weak-form given in Equation (4). The displacement $\mathbf{u}$ for a point $\mathbf{x}$ in the meshfree domain can be approximated by

$$\mathbf{u}_{(\mathrm{MM})}(\mathbf{x}) = \sum_{i=1}^{n} \boldsymbol{\Phi}_i(\mathbf{x}) \mathbf{u}_i \tag{5}$$

where $\boldsymbol{\Phi}$ is the matrix for the meshfree shape functions, and n is the number of field nodes selected in the local interpolation domain. Several methods have been developed for the construction of the meshfree shape functions (Liu and Gu, 2005), e.g., the moving least squares approximation (MLSA), the radial point interpolation method (RPIM), the Kriging interpolation (Wang et al., 2003), etc. Due to the robustness, the moving least squares approximation (MLSA) is used in this paper.

The interpolation formulation of FEM can be written as (Zienkiewicz and Taylor, 2000)

$$\mathbf{u}(\mathbf{x}) = \sum_{i=1}^{n_e} \mathbf{N}_i(\mathbf{x}) \mathbf{u}_i \qquad n_e=3,4,5,\ldots.. \tag{6}$$

where n_{e} is the number of nodes in a FE element, and $\mathbf{N}$ is the matrix of the FE shape functions.

Substituting the expression of displacement $\mathbf{u}$ given in Equations (5) and (6) into Equation (4), and using the stationary condition for Equation (4) yields

$$\mathbf{K}_{(\mathrm{FE})} \mathbf{U}_{(\mathrm{FE})} = \mathbf{F}_{(\mathrm{FE})} \tag{7}$$

$$\mathbf{K}_{(\mathrm{MM})} \mathbf{U}_{(\mathrm{MM})} = \mathbf{F}_{(\mathrm{MM})} \tag{8}$$

where $\mathbf{K}_{(\mathrm{FE})}$, $\mathbf{U}_{(\mathrm{FE})}$, $\mathbf{F}_{(\mathrm{FE})}$, $\mathbf{K}_{(\mathrm{MM})}$, $\mathbf{U}_{(\mathrm{MM})}$, and $\mathbf{F}_{(\mathrm{MM})}$ are stiffness matrices, the displacement vectors, and the force vectors for FEM and the meshfree method, respectively. We have

$$\mathbf{K}_{(\mathrm{FE})ij} = \int_{\Omega} \mathbf{B}_{(\mathrm{FE})i}{}^{\mathrm{T}} \mathbf{D} \mathbf{B}_{(\mathrm{FE})j} \mathrm{d}\Omega \tag{9}$$

$$\mathbf{K}_{(\mathrm{MM})ij} = \int_{\Omega} \mathbf{B}_{(\mathrm{MM})i}{}^{\mathrm{T}} \mathbf{D} \mathbf{B}_{(\mathrm{MM})j} \mathrm{d}\Omega \tag{10}$$

$$\mathbf{F}_{(\mathrm{FE})i} = \int_{\Gamma_t} N_i \bar{\mathbf{t}} \mathrm{d}\Gamma + \int_{\Omega} N_i \mathbf{b} \mathrm{d}\Omega \tag{11}$$

$$\mathbf{F}_{(\mathrm{MM})i} = \int_{\Gamma_t} \Phi_i \bar{\mathbf{t}} \mathrm{d}\Gamma + \int_{\Omega} \Phi_i \mathbf{b} \mathrm{d}\Omega \tag{12}$$

where $\mathbf{D}$ is the matrix of material constants, and

Comput Mech (2009) 44:119–131
DOI 10.1007/s00466-008-0359-y

$$\mathbf{B}_{(\mathrm{FE})i} = \begin{bmatrix} N_{i,x} & 0 \\ 0 & N_{i,y} \\ N_{i,y} & N_{i,x} \end{bmatrix}, \qquad \mathbf{B}_{(\mathrm{MM})i} = \begin{bmatrix} \phi_{i,x} & 0 \\ 0 & \phi_{i,y} \\ \phi_{i,y} & \phi_{i,x} \end{bmatrix} \tag{13}$$

3 Coupling of the meshfree method and FEM by the bridging transition technique

3.1 The combination condition

As shown in Figure 1, consider a 2D problem domain. A sub-domain, $\Omega_{(\mathrm{MM})}$, is represented by the meshfree nodes and the other sub-domain, $\Omega_{(\mathrm{FE})}$, is discretized by FEM mesh. These two domains are joined together by a transition (bridging) domain $\Omega_{(\mathrm{T})}$ which possesses displacement compatibility and force equilibrium in coupling $\Omega_{(\mathrm{MM})}$ and $\Omega_{(\mathrm{FEM})}$, i.e.,

$$\mathbf{u}_{(\mathrm{MM})k} = \mathbf{u}_{(\mathrm{FE})k} \tag{14}$$

$$\mathbf{f}_{(\mathrm{MM})k} + \mathbf{f}_{(\mathrm{FE})k} = 0 \tag{15}$$

where $\mathbf{u}_{(\mathrm{MM})k}$, $\mathbf{u}_{(\mathrm{FE})k}$, $\mathbf{f}_{(\mathrm{MM})k}$ and $\mathbf{f}_{(\mathrm{FE})k}$ are displacements and forces at a transition particle k obtained by the meshfree method in $\Omega_{(\mathrm{MM})}$ and FEM in $\Omega_{(\mathrm{FE})}$, respectively.

It will be ideal to satisfy both the displacement compatibility and the force equilibrium conditions at the same time, in which the displacement compatibility Equation (14) is the most important and must be satisfied. However, because the meshfree MLSA shape functions lack the delta function properties, it is difficult to directly satisfy the compatibility in the connection of these two domains.

To satisfy the displacement compatibility condition, two combination techniques: a) using the hybrid displacement shape function algorithm (Belytschko and Organ, 1995; Gu and Liu, 2001c), and b) using the modified variational form algorithm (Hegen, 1996; Gu and Liu, 2003) have been developed. In these two techniques, two different domains are connected through a common boundary (e.g., a curve for a 2D problem and a surface for a 3D problem), as shown in Figures 1 and 2, called the interface, Γ_I. The interface boundary is discretized by meshfree nodes and the FEM nodes which coincide (have the same space positions) with each other. We will briefly review these two techniques in the following part.

Combination technique 1: using FE interface elements and hybrid displacement shape function

This method is to introduce finite element (FE) interface elements in the meshfree domain, in which the MLSA shape functions are used, near the interface boundary Γ_I. In a FE

Comput Mech (2009) 44:119–131
DOI 10.1007/s00466-008-0359-y

interface element, a hybrid displacement approximation is defined so that the MLSA shape functions in the meshfree domain along Γ_I possess the delta function property.

A detailed figure of the interface domain is shown in Figure 2. Ω_I is a layer of FE interface elements along the interface boundary Γ_I within the meshfree domain $\Omega_{(MM)}$. The new displacement approximation in these FE interface elements can be re-written as:

$$u_1^h(\mathbf{x}) = \sum_{i=1}^{n} \tilde{\Phi}_i(\mathbf{x}) u_i \tag{16}$$

where the hybrid shape functions (Belytschko and Organ, 1995)of the interface element are defined as

$$\tilde{\Phi}_i(\mathbf{x}) = \begin{cases} (1-R(\mathbf{x}))\Phi_i(\mathbf{x}) + R(\mathbf{x})N_i(x) & \mathbf{x} \in \Omega_I \\ \Phi_i(\mathbf{x}) & \mathbf{x} \in \Omega_{(MM)} - \Omega_I \end{cases} \tag{17}$$

The ramp function R equals to the summation of the FE shape functions of an FE interface element associated with interface element nodes that are located on the interface boundary Γ_I, i.e.

$$R(\mathbf{x}) = \sum_{i=1}^{n} N_i(\mathbf{x}) = \begin{cases} 1 & \mathbf{x} \in \Gamma_I \\ 0 & \mathbf{x} \in \Omega_{(MM)} - \Omega_I \end{cases}, \quad x_i \in \Gamma_I \tag{18}$$

where n is the number of FE nodes located on the interface boundary Γ_I for an interface element. According to the property of FE shape functions, R will be unity along Γ_I and vanish outside of the interface domain.

It has been found (Belytschko and Organ, 1995; Gu and Liu, 2001c) that the displacement approximation is continuous from the purely meshfree domain ($\Omega_{(MM)}$-Ω_I) passing to the interface domain Ω_I. The derivative of the hybrid shape function is, however, discontinuous across the interface boundary. Hence, the stress calculated will not be continuous across the interface resulting in the error in using this coupled method.

Combination technique 2: using modified variational form

In some coupled methods (e.g. EFG/FEM, etc.) (Hegen,1996; Gu and Liu, 2003), the similar weak forms (functional forms) are used in both of numerical methods. The modified variational form can be used in these coupled methods. Consider the above discussed coupled 2D problem, a sub-functional Π_I can be introduced to enforce the compatibility condition of Equation (14) by means of Lagrange multiplier $\boldsymbol{\gamma}$ on the interface boundary

Comput Mech (2009) 44:119–131
DOI 10.1007/s00466-008-0359-y

$$\Pi_{\mathrm{I}} = \int_{\Gamma_{\mathrm{I}}} \boldsymbol{\gamma} \cdot (\tilde{\mathbf{u}}_{(\mathrm{FEM})I} - \tilde{\mathbf{u}}_{(\mathrm{MM})I}) \mathrm{d}\Gamma = \int_{\Gamma_{\mathrm{I}}} \boldsymbol{\gamma} \tilde{\mathbf{u}}_{(\mathrm{FEM})I} \mathrm{d}\Gamma - \int_{\Gamma_{\mathrm{I}}} \boldsymbol{\gamma} \tilde{\mathbf{u}}_{(\mathrm{MM})I} \mathrm{d}\Gamma$$
$$= \Pi_{(\mathrm{FEM})\mathrm{I}} - \Pi_{(\mathrm{MM})\mathrm{I}} \tag{19}$$

In the above equation, $\Pi_{(\mathrm{FEM})\mathrm{I}}$ and $\Pi_{(\mathrm{MM})\mathrm{I}}$ are the boundary integrations along the interface boundary, Γ_{I}, in FEM and meshfree domains. Introducing $\Pi_{(\mathrm{FEM})\mathrm{I}}$ and $\Pi_{(\mathrm{MM})\mathrm{I}}$ given in Equation (19) separately into functional forms of FEM and MM given in Equation (4) to get generalized functional forms for them. Therefore, the different sub-domains can be connected via Lagrange multipliers, $\boldsymbol{\gamma}$.

In summary, the above discussed two techniques have been used in the development of several coupled methods including the EFG/FEM/BEM and MLPG/FEM/BEM (Gu and Liu, 2003; Liu and Gu, 2000a,b). However, in these two techniques, a common interface boundary is used between FEM domain, $\Omega_{(\mathrm{FE})}$, and the meshfree domain, $\Omega_{(\mathrm{MM})}$. They have inherent shortcomings including: i) it is very difficult to ensure the high-order compatibility through this interface boundary; ii) because the meshfree nodes and the FEM nodes along this interface boundary coincide with each other, and are dependent on each other, it will increase the cost in "meshing" work, especially for some problems with complex interface boundaries.

3.2 The bridging transition technique

To overcome the shortcomings of the traditional combination techniques which have been discussed in previous section, a novel bridging transition technique is developed. As shown in Figure 3, a problem domain is divided into meshfree domain, $\Omega_{(\mathrm{MM})}$ and FEM domain, $\Omega_{(\mathrm{FE})}$, but these two domains are joined by a transition (bridging) domain $\Omega_{(\mathrm{T})}$ which is not an interface boundary but a region instead.

The generalized displacement at a point $\mathbf{x}$ in the transition domain can be defined as

$$\mathbf{g}(\mathbf{x}) = \mathbf{u}_{(\mathrm{MM})}(\mathbf{x}) - \mathbf{u}_{(\mathbf{FE})}(\mathbf{x}) \tag{20}$$

where $\mathbf{u}_{(\mathrm{MM})}(\mathbf{x})$ and $\mathbf{u}_{(\mathrm{FE})}(\mathbf{x})$ are the displacements at the point $\mathbf{x}$, obtained by the interpolations using the meshfree nodes and the FEM element, respectively, i.e.,

$$\mathbf{u}_{(\mathrm{MM})}(\mathbf{x}) = \sum_I \boldsymbol{\Phi}_I(\mathbf{x}) \mathbf{u}_{(\mathrm{MM})I} \tag{21}$$

$$\mathbf{u}_{(\mathrm{FE})}(\mathbf{x}) = \sum_J \mathbf{N}_J(\mathbf{x}) \mathbf{u}_{(\mathrm{FE})J} \tag{22}$$

A discretized sub-functional is introduced to enforce the displacement compatibility condition given in Equation (14) by means of Lagrange multiplier λ in the transition domain

Comput Mech (2009) 44:119–131
DOI 10.1007/s00466-008-0359-y

$$\begin{aligned}\Pi_{(\mathrm{T})} &= \int_{\Omega_{(\mathrm{T})}} \boldsymbol{\lambda}\cdot\mathbf{g}\mathrm{d}\Omega = \int_{\Omega_{(\mathrm{T})}} \boldsymbol{\lambda}\cdot\left[\mathbf{u}_{(\mathrm{MM})}-\mathbf{u}_{(\mathrm{FE})}\right]\mathrm{d}\Omega \\ &= \int_{\Omega_{(\mathrm{T})}} \boldsymbol{\lambda}\cdot\mathbf{u}_{(\mathrm{MM})}\mathrm{d}\Omega - \int_{\Omega_{(\mathrm{T})}} \boldsymbol{\lambda}\cdot\mathbf{u}_{(\mathrm{FE})}\mathrm{d}\Omega \\ &= \Pi_{(\mathrm{T})}^{(\mathrm{MM})} - \Pi_{(\mathrm{T})}^{(\mathrm{FE})}\end{aligned} \tag{23}$$

In which, $\Pi_{(\mathrm{T})}^{(\mathrm{MM})}$ and $\Pi_{(\mathrm{T})}^{(\mathrm{FE})}$ are the sub-functional for the meshfree part and the FEM part. Substituting $\Pi_{(\mathrm{T})}^{(\mathrm{MM})}$ and $\Pi_{(\mathrm{T})}^{(\mathrm{FE})}$ separately into Equation (4) for the meshfree method and FEM, generalized functional forms can be written as

$$\Pi_{(\mathrm{MM})} = \int_{\Omega_{(\mathrm{MM})}} \frac{1}{2}\boldsymbol{\varepsilon}^{\mathrm{T}}\cdot\boldsymbol{\sigma}\mathrm{d}\Omega - \int_{\Omega_{(\mathrm{MM})}} \mathbf{u}^{\mathrm{T}}\cdot\mathbf{b}\mathrm{d}\Omega - \int_{\Gamma_{(\mathrm{MM})^t}} \mathbf{u}^{\mathrm{T}}\cdot\bar{\mathbf{t}}\mathrm{d}\Gamma + \int_{\Omega_{(\mathrm{T})}} \boldsymbol{\lambda}\cdot\mathbf{u}_{(\mathrm{MM})}\mathrm{d}\Omega \tag{24}$$

$$\Pi_{(\mathrm{FE})} = \int_{\Omega_{(\mathrm{FE})}} \frac{1}{2}\boldsymbol{\varepsilon}^{\mathrm{T}}\cdot\boldsymbol{\sigma}\mathrm{d}\Omega - \int_{\Omega_{(\mathrm{FE})}} \mathbf{u}^{\mathrm{T}}\cdot\mathbf{b}\mathrm{d}\Omega - \int_{\Gamma_{(\mathrm{FE})^t}} \mathbf{u}^{\mathrm{T}}\cdot\bar{\mathbf{t}}\mathrm{d}\Gamma - \int_{\Omega_{(\mathrm{T})}} \boldsymbol{\lambda}\cdot\mathbf{u}_{(\mathrm{FE})}\mathrm{d}\Omega \tag{25}$$

In these variational formulations, the domains of $\Omega_{(\mathrm{FE})}$ and $\Omega_{(\mathrm{MM})}$.are connected via Lagrange multiplier $\boldsymbol{\lambda}$, which can be given by the interpolation functions $\boldsymbol{\Lambda}$ and the nodal value of $\boldsymbol{\lambda}_i$

$$\boldsymbol{\lambda}(\mathbf{x}) = \sum_i \Lambda_i(\mathbf{x})\cdot\boldsymbol{\lambda}_i \tag{26}$$

$\boldsymbol{\Lambda}$ is the selected interpolation function for $\boldsymbol{\lambda}_i$ and it can use the FEM shape function.

Substituting Equations (5), (21) and (26) into Equation (24), and using the stationary condition based on the displacement, the following modified meshfree equations can be obtained

$$\left[\mathbf{K}_{(\mathrm{MM})} \quad \mathbf{B}_{(\mathrm{MM})}\right]\begin{Bmatrix}\mathbf{U}_{(\mathrm{MM})}\\ \boldsymbol{\lambda}\end{Bmatrix} = \left\{\mathbf{F}_{(\mathrm{MM})}\right\} \tag{27}$$

where $\mathbf{K}_{(\mathrm{MM})}$ and $\mathbf{F}_{(\mathrm{MM})}$ have been defined in Equations (10) and (12), $\mathbf{B}_{(\mathrm{MM})}$ is defined as

$$\mathbf{B}_{(\mathrm{MM})} = \int_{\Omega_{(\mathrm{T})}} \boldsymbol{\Lambda}\boldsymbol{\Phi}^{\mathrm{T}}\mathrm{d}\Omega, \tag{28}$$

Substituting Equations (6), (21) and (26) into Equation (25), and using the stationary condition based on the displacement, lead to the following modified FEM equations

$$\left[\mathbf{K}_{(\mathrm{FE})} \quad -\mathbf{B}_{(\mathrm{FE})}\right]\begin{Bmatrix}\mathbf{U}_{(\mathrm{FE})}\\ \boldsymbol{\lambda}\end{Bmatrix} = \left\{\mathbf{F}_{(\mathrm{FE})}\right\} \tag{29}$$

where $\mathbf{K}_{(\mathrm{FE})}$ and $\mathbf{F}_{(\mathrm{FE})}$ have been defined in Equations (9) and (11), $\mathbf{B}_{(\mathrm{FE})}$ is defined as

$$\mathbf{B}_{(\mathrm{FE})} = \int_{\Omega_{(\mathrm{T})}} \boldsymbol{\Lambda}\mathbf{N}^{\mathrm{T}}\mathrm{d}\Omega \tag{30}$$

Comput Mech (2009) 44:119–131
DOI 10.1007/s00466-008-0359-y

To get $\mathbf{B}_{(\mathrm{MM})}$ and $\mathbf{B}_{(\mathrm{FEM})}$ numerically, the transition domain should be divided into several regular cells for the Gauss numerical integration. In addition, it should be mentioned here that to ensure the conservations of mass and energy, the energy and mass (for the dynamic problem) for MM and FE in the transition region can be taken to be linear or constant distributions (Xiao and Belytschko, 2004).

It is impossible to solve Equations (27) and (29) separately. Using the stationary condition of Equations (27) and (29) based on the Lagrange multiplier and considering the compatibility condition, we can obtain the relationship, i.e.,

$$\mathbf{B}^T_{(\mathrm{MM})}\mathbf{U}_{(\mathrm{MM})} - \mathbf{B}^T_{(\mathrm{FE})}\mathbf{U}_{(\mathbf{FE})} = \mathbf{0} \tag{31}$$

Because two domains are connected through the transition domain, assembling of Equations (27), (29) and (31) yields the following linear system of equations

$$\begin{bmatrix} \mathbf{K}_{(\mathrm{MM})} & \mathbf{0} & \mathbf{B}_{(\mathrm{MM})} \\ \mathbf{0} & \mathbf{K}_{(\mathrm{FE})} & -\mathbf{B}_{(\mathrm{FE})} \\ \mathbf{B}^T_{(\mathrm{MM})} & -\mathbf{B}^T_{(\mathrm{FE})} & \mathbf{0} \end{bmatrix} \begin{Bmatrix} \mathbf{U}_{(\mathrm{MM})} \\ \mathbf{U}_{(\mathbf{FE})} \\ \boldsymbol{\lambda} \end{Bmatrix} = \begin{Bmatrix} \mathbf{F}_{(\mathrm{MM})} \\ \mathbf{F}_{(\mathrm{FE})} \\ \mathbf{0} \end{Bmatrix} \tag{32}$$

Solving Equation (32) together with the displacement boundary conditions, given in Equation (2) , we can obtain the solution for the problem considered.

To satisfy the force equilibrium condition, the generalized derivative at a point $\mathbf{x}$ in the transition domain can be written as

$$\mathbf{g}_{,x}(\mathbf{x}) = \frac{\partial \mathbf{u}_{(\mathrm{MM})}(\mathbf{x})}{\partial \mathbf{x}} - \frac{\partial \mathbf{u}_{(\mathrm{FE})}(\mathbf{x})}{\partial \mathbf{x}} \tag{33}$$

and using Lagrange multiplier γ

$$\begin{aligned} \Pi_{(\mathrm{T})(\mathbf{x})} &= \int_{\Omega_{(\mathrm{T})k}} \boldsymbol{\gamma} \cdot \mathbf{g}_{,\mathbf{x}} \mathrm{d}\Omega \\ &= \int_{\Omega_{(\mathrm{T})}} \boldsymbol{\gamma} \cdot \frac{\partial \mathbf{u}_{(\mathrm{MM})}(\mathbf{x})}{\partial \mathbf{x}} \mathrm{d}\Omega - \int_{\Omega_{(\mathrm{T})}} \boldsymbol{\gamma} \cdot \frac{\partial \mathbf{u}_{(\mathrm{FE})}(\mathbf{x})}{\partial \mathbf{x}} \mathrm{d}\Omega \\ &= \Pi^{(\mathrm{MM})}_{(\mathrm{T})(\mathbf{x})} - \Pi^{(\mathrm{FE})}_{(\mathrm{T})(\mathbf{x})} \end{aligned} \tag{34}$$

Following the similar procedure from Equation (24) to Equation (32), we can obtain the coupling equations to satisfy the high-order compatibility

$$\begin{bmatrix} \mathbf{K}_{(\mathrm{MM})} & \mathbf{0} & \mathbf{B}_{(\mathrm{MM})} & \mathbf{A}_{(\mathrm{MM})} \\ \mathbf{0} & \mathbf{K}_{(\mathrm{FE})} & -\mathbf{B}_{(\mathrm{FE})} & -\mathbf{A}_{(\mathrm{FE})} \\ \mathbf{B}^T_{(\mathrm{MM})} & -\mathbf{B}^T_{(\mathrm{FE})} & \mathbf{0} & \mathbf{0} \\ \mathbf{A}^T_{(\mathrm{MM})} & -\mathbf{A}^T_{(\mathrm{FE})} & \mathbf{0} & \mathbf{0} \end{bmatrix} \begin{Bmatrix} \mathbf{U}_{(\mathrm{MM})} \\ \mathbf{U}_{(\mathbf{FE})} \\ \boldsymbol{\lambda} \\ \boldsymbol{\gamma} \end{Bmatrix} = \begin{Bmatrix} \mathbf{F}_{(\mathrm{MM})} \\ \mathbf{F}_{(\mathrm{FE})} \\ \mathbf{0} \\ \mathbf{0} \end{Bmatrix} \tag{35}$$

where

Comput Mech (2009) 44:119–131
DOI 10.1007/s00466-008-0359-y

$$\mathbf{A}_{(\mathrm{MM})} = \int_{\Omega_{(\mathrm{T})}} \boldsymbol{\Psi} \frac{\partial \boldsymbol{\Phi}^{\mathrm{T}}}{\partial \mathbf{x}} \mathrm{d}\Omega, \tag{36}$$

$$\mathbf{A}_{(\mathrm{FE})} = \int_{\Omega_{(\mathrm{T})}} \boldsymbol{\Psi} \frac{\partial \mathbf{N}^{\mathrm{T}}}{\partial \mathbf{x}} \mathrm{d}\Omega \tag{37}$$

where $\boldsymbol{\Psi}$ is the interpolation functions for $\boldsymbol{\gamma}$.

In the practical computation, to simplify the integration and reduce the "meshing" cost, several layers of transition particles, which are usually regularly distributed, can be inserted into the transition domain $\Omega_{(\mathrm{T})}$. The displacement compatibility between FEM and meshfree domains is achieved through these transition particles. Using these transition particles, **B** and **A** in Equations (28), (30), (36), and (37) can be re-written as:

$$\mathbf{B}_{(\mathrm{MM})} = \sum_{k=1}^{m} \boldsymbol{\Lambda} \boldsymbol{\Phi}^{\mathrm{T}} \tag{38}$$

$$\mathbf{B}_{(\mathrm{FE})} = \sum_{k=1}^{m} \boldsymbol{\Lambda} \mathbf{N}^{\mathrm{T}} \tag{39}$$

$$\mathbf{A}_{(\mathrm{MM})} = \sum_{k=1}^{m} \boldsymbol{\Psi} \frac{\partial \boldsymbol{\Phi}^{\mathrm{T}}}{\partial \mathbf{x}}, \tag{40}$$

$$\mathbf{A}_{(\mathrm{FE})} = \sum_{k=1}^{m} \boldsymbol{\Psi} \frac{\partial \mathbf{N}^{\mathrm{T}}}{\partial \mathbf{x}} \tag{41}$$

where m is the number of the transition particles. It should be mentioned that using the transition particles to replace the numerical integration will decrease the computational accuracy. However, it will significantly improve the computational efficiency comparing with using the Gauss numerical integrations.

The above developed Lagrange multiplier method is accurate and the physical meaning of Lagrange multipliers is also very clear. Physically, the Lagrange multiplier is a general force in the transition region generated because of the incompatibility of displacement or force. However, it will increase the computational cost (especially when the bridging domain becomes large) because new variables (Lagrange multipliers) are added in the system of equations. Hence, we can use the modified Lagrange multipliers to yield the so-called penalty method, i.e., the general Lagrange multiplier method can be used to obtain a range of penalty coefficients, and then use these penalty coefficients as constants for this problem and other similar problems to save computational cost.

The advantages of using the above presented bridging transition technique include:

1) it allows the meshfree nodes in $\Omega_{(MM)}$ to have an arbitrary distribution and become independent of the distributions of the FEM nodes in $\Omega_{(FE)}$. Hence, the mesh- and node-generation become easy and cheap;

2) the compatibility conditions in the transition domain can be conveniently controlled through adjusting the number and distribution of the transition particles. For some sub-transition domains with higher compatibility requirement, a finer transition particle distribution can be used;

3) the compatibility of higher order derivatives can be satisfied. It will be very benefit to improve the accuracy for stress field.

Hence, the bridging transition technique is more effective than the old transition techniques which have been discussed in Section 3.1.

However, it should be mentioned here that the size of transition region and the distributions of transition particles will affect the performance of this coupled method. There are no theoretical best values for these two parameters, and the numerical studies can be used to get the reasonable values. In the following section, we will numerically investigate and recommend some values for the size of transition region and the distribution of the transition particles.

4 Numerical results

Several cases of two-dimensional solids and structures have been studied in order to examine the performance of the present coupled MM/FE method using the bridging transition technique, because 2D cases are convenient and usually sufficient to explore the properties and performance for a newly developed numerical technique. Except when mentioned, the units are taken as standard international (SI) units in the following examples. In most cases, sixteen field nodes, which are the closest to the interpolation point, are used to construct the meshless shape functions.

4.1 Cantilever beam

A two-dimensional cantilever beam problem is firstly used to verify the coupled method, because its' analytical solution is available and can be found in the textbook by Timoshenko and Goodier (1970). This problem has been widely studied by many numerical methods including the meshfree methods, so it is convenient to compare the new developed coupled method with other methods. Consider a 2D beam, as shown in Figure 4, with length L=48 and height D=12 subjected to a parabolic traction, P=1000, at the free end. The beam has a unit

thickness and a plane stress problem is considered. The material parameters of it are taken as E=3.0×10^7 and ν=0.3.

As shown in Figure 5, the beam is divided into two parts. FEM using the triangular elements is used for the left part where the essential boundary condition is included. The meshfree method is used for the right part where the traction boundary condition is applied. These two parts are connected through a transition region that is discretized by 54 (9×6) regularly distributed transition particles.

The displacement results obtained by the coupled method are compared with the analytical solution. It has been found that they agree very well. Figure 6 illustrates the comparison between the shear stress calculated analytically and by the coupled method at the section of x=L/2. The plot shows an excellent agreement between the analytical and numerical results. In addition, from this figure, we can also see that the new bridging transition technique can ensure the high-order continuity of stresses between the FEM domain and the MM domain.

As above mentioned, several parameters significantly affect the performance of this newly developed coupled method. These parameters will be studied in following part. For quantitative error studies, we define the following norm using shear stresses as an error indicator, as the accuracy of shear strain or shear stress is much more critical for this beam problem.

$$e_t = \frac{1}{N}\sqrt{\sum_{i=1}^{N}(\tau_i - \bar{\tau}_i)^2 \Big/ \sum_{i=1}^{N}\bar{\tau}^2} \tag{42}$$

where N is the number of nodes investigated, τ is the shear stress obtained by numerical method, and $\bar{\tau}$ is the analytical shear stress. The displacement fields have been obtained by MM/FEM, FEM and pure meshfree method, and their results are almost identical. Therefore, for quantificational error studies, we only present the results for stress errors in the following studies.

a) Influence of the size of transition region

The size of transition (bridging) region will affect the performance of the coupled method. The size, d_t, of transition region is defined as:

$$d_t = \alpha \cdot d_{FE} \text{ or } d_t = \alpha \cdot d_{MM} \tag{43}$$

where α is a dimensionless parameter, d_{FE} and d_{MM} are equivalent sizes of FEM element and meshfree nodal space, respectively. For this beam problem, d_{FE} and d_{MM} are nearly same, so we can use either d_{FE} or d_{MM} in Equation (43).

Figure 7 plots the computational errors vs. the dimensionless parameter α. From this figure, we can find that the transition region should be large enough to ensure the compatibility. If the size is too small, it will decrease the transition accuracy, especially for the high order compatibility. However, if the size is too big, it will significantly increase the computational cost without further improvement of computational accuracy. In other word, if the size of the transition region is large enough, the numerical results is not sensitive to this size. From our studies for the beam problem, we have found that it is reasonable to use $\alpha = 3 \sim 5$.

b) Influence of the distribution of transition particle

To investigate the influence of the transition particles, we use the uniformly distributed transition particles and the equivalent transition particle space, d_p, is defined as

$$d_p = \beta \cdot d_{FE} \text{ or } d_p = \beta \cdot d_{MM} \tag{44}$$

where β is a dimensionless parameter.

The errors for different distributions of transition particles are illustrated in Figure 8, where we can see that the computational results are stable when the particle space is small enough ($\beta \le 1.0$ for this problem). Too few transition particles cannot ensure the compatibility, and therefore lead to a large computational error. On the other hand, if the transition particles are too many, it will significantly increase the computational cost without noticeable accuracy improvement. Hence, the number of transition particles should be considered to maximize the computation efficiency with acceptable accuracy. For the present study, $0.2 \le \beta \le 1.0$ is a good choice.

In order to explore the influence of the replacement of numerical integration by the transition particles, the transition region is also divided into 40 (8×5) integration cells and 16(4×4) Gauss points are used for each cell. The Gauss numerical integration is used to calculate matrixes of **A** and **B** using Equations (28), (30), (36) and (37). It has been found although the numerical integration method has better (about 10% better) computational accuracy than the transition particle method, it needs much more computational cost (the CPU time is almost double) than the transition particle method. Hence, using the transition particle method is more effective than the numerical integration method.

However, it should be mentioned here that the above conclusion of the transition particle method with better computational efficiency is drawn through comparing with Gauss numerical integration scheme which is widely used in FEM and meshless methods. Actually, many other numerical integration schemes are available. If a suitable specific numerical integration scheme is employed, the transition particle method may not be the optimal choice for the considered situation.

c) The numerical stability and convergence study

The numerical stabilities of FEM and the meshfree method have been thoroughly studied (Zienkiewicz and Taylor,2000; Liu,2002, 2008). When the equivalent nodal space in the meshfree domain is close to the FEM element size, the condition numbers of $\mathbf{K}_{(FE)}$ and $\mathbf{K}_{(MM)}$ are also close. However, in a coupled method, the present of the extra items in the weak form (e.g., Equation (19)) for enforcement of compatibility in the transition region will increase the condition number of the final coefficient matrix. Regarding to the numerical stability, the newly developed coupled method has the similar property as common coupled methods. Fortunately, from our study, we have found that if $\alpha = 3 \sim 5$ and $\beta \approx 1.0$ are used in this new coupled method, the increase of condition number is not significant and it is better than the normal coupled methods discussed in Section 3.1. Hence, the newly developed coupled method has the better numerical stability than the normal coupled methods.

Using the recommended parameters, the convergence with different nodal discretizations is studied and shown in Figure 9, where h is equivalent FEM element size in this case. It is observed that the convergence of the present coupled method is good. The convergence of the pure meshfree method for this problem is also plotted in the same figure. It can be found from this figure that the accuracy of the new presented coupled method is slightly worse than that of the pure meshfree method. However, the convergence rates of these two techniques are nearly same. It is because that the accuracy of the meshfree method plays the important role for the convergence rates in this coupled technique.

4.2 Hole in an infinite plate

A plate with a circular hole subjected to a unidirectional tensile load of 1.0 in the x direction is considered. Due to symmetry, only the upper right quadrant (size 10×10) of the plate is modeled as shown in Figure 10. When the condition $b/a>5$ is satisfied, the solution of finite plate is closed to that of the infinite plate (Timoshenko and Goodier, 1970). Plane strain condition is assumed, and $E=1.0\times10^3$, $\nu=0.3$. Symmetry conditions are imposed on the left

Comput Mech (2009) 44:119–131
DOI 10.1007/s00466-008-0359-y

and bottom edges, and the inner boundary of the hole is traction free. The tensile load in the x direction is imposed on the right edge. The exact solution for the stresses of infinite plate is

$$\sigma_x(x,y) = 1 - \frac{a^2}{r^2}\{\frac{3}{2}\cos 2\theta + \cos 4\theta\} + \frac{3a^4}{2r^4}\cos 4\theta \tag{45}$$

$$\sigma_y(x,y) = -\frac{a^2}{r^2}\{\frac{1}{2}\cos 2\theta - \cos 4\theta\} - \frac{3a^4}{2r^4}\cos 4\theta \tag{46}$$

$$\sigma_{xy}(x,y) = -\frac{a^2}{r^2}\{\frac{1}{2}\sin 2\theta + \sin 4\theta\} + \frac{3a^4}{2r^4}\sin 4\theta \tag{47}$$

where (r,θ) are the polar coordinates and θ is measured counter-clockwise from the positive x axis.

As shown in Figure 11, the plate is divided into two domains, where the meshfree method and FEM are applied, respectively. As the stress is most critical, detailed results on stress are presented here. The stress σ_x at x=0 obtained by the coupled method is plotted in Figure 12. It can be observed that the coupled method yields satisfactory results for the problem considered. Again, we can also see that the new coupled method can ensure the high-order continuity of stresses between the FEM domain and the MM domain.

4.3 A cracked plate

A well-known near-tip field, which is subjected to mode-I displacement field (Ching and Batra, 2001) at its edges, is analyzed. As shown in Figure 13, an edge-cracked square plate is subjected to the following displacement field for a model-I crack (Anderson, 1991).

$$\begin{Bmatrix} u \\ v \end{Bmatrix} = \frac{K_I}{2\mu}\sqrt{\frac{r}{2\pi}} \begin{Bmatrix} \cos\frac{\theta}{2}\left[\kappa - 1 + 2\sin^2\frac{\theta}{2}\right] \\ \sin\frac{\theta}{2}\left[\kappa + 1 - 2\cos^2\frac{\theta}{2}\right] \end{Bmatrix} \tag{48}$$

where K_I is the stress intensity factors for mode-I dependent upon the crack length, the specimen geometry and the applied loading, and (r, θ) are the cylindrical coordinates of a point with the origin located at the crack-tip and the positive angle measured counterclockwise from the axis of the crack. Hence, the analytical solution for the stress field is given

Comput Mech (2009) 44:119–131
DOI 10.1007/s00466-008-0359-y

$$\begin{Bmatrix}\sigma_{11}\\ \sigma_{22}\\ \sigma_{12}\end{Bmatrix}=\frac{K_I}{\sqrt{2\pi r}}\cos\frac{\theta}{2}\begin{Bmatrix}1-\sin\frac{\theta}{2}\sin\frac{3\theta}{2}\\ 1+\sin\frac{\theta}{2}\sin\frac{3\theta}{2}\\ \sin\frac{\theta}{2}\sin\frac{3\theta}{2}\end{Bmatrix} \tag{49}$$

The plate is divided into two parts: the meshfree method is used for the central part, in which the crack embedded, and FEM is used for other parts. The computational model is plotted in Figure 14. Figure 15 shows the stress distribution along the crack axis (when θ=0°). Clearly, the prediction of the newly developed coupled method matches the analytical solution very well.

4.4 A complex plate with a hole

A complexly shaped plate with a "C" shaped hole is studied. One edge of this plate is fixed, one edge is subjected to uniformly distributed tension load, and other edges are traction free. The material parameters of it are taken as E=3.0×10^7 and ν=0.3.

There should be stress concentration around the hole. Hence, as shown in Figure 16, the plate is divided into two parts. The meshfree method is used in the central part including the hole, and FEM is used for other parts. The computational model is also plotted in Figure 16. In the transition region, 560 regularly distributed transition particles are used. As the reference solution, this problem is also analyzed by the pure meshfree method (the software of MFree 2D: Liu, 2002) with very fine nodal distribution. Figures 17 and 18 show the distribution of stress, σ_{xx} and σ_{yy}. They are almost identical with the pure meshfree method result. The coupled analysis obtained the maximum σ_{xx} =3.4 (at the lower corner of the hole), which only has less than 5% difference with the pure meshfree results.

It should be mentioned here that because the size of whole computational domain for this problem is much larger than that of the hole, it will need a large number of nodes if it is simulated by a pure meshfree method. The coupled method is more effective for this problem because it uses meshfree simulation around the hole to accurately capture the stress field, and FEM is used in other regions to improve the computational efficiency.

5 Conclusions

A bridging transition technique, which is a totally new technique comparing with the existing combination techniques, is developed for coupling the meshfree method (MM) with

Comput Mech (2009) 44:119–131
DOI 10.1007/s00466-008-0359-y

the finite element method (FEM). The transition from the meshfree to finite element (FE) domains is realized by a transition (bridging) region, and the Lagrange multiplier method is used to ensure the compatibility of displacements and their gradients in the transition region. For simplification, regularly distributed transition particles, which are independent of either the meshfree nodes or the FE nodes, can be inserted into the transition region to avoid the numerical integration and to improve the flexibility. Numerical examples have demonstrated effectiveness of the present coupled method for solid and structure problems.

The following conclusions can be drawn through the studies in this paper.

a) The size of transition (bridging) region will affect the performance of the coupled method. The transition region should be large enough to ensure the compatibility, but it should not be too large to save computational cost. $\alpha = 3 \sim 5$ is recommended for most of problems.

b) Using the transition particles to replace the numerical integration will save computational cost, although the accuracy will slightly decrease. Too few transition particles cannot ensure the compatibility accuracy, but too many transition particles will significantly increase the computational cost without noticeable accuracy improvement. $0.2 \le \beta \le 1.0$ is a good choice.

c) If $\alpha = 3 \sim 5$ and $\beta \approx 1.0$, the coupled method will not significantly increase the condition number of the final coefficient matrix. The newly developed coupled method has good numerical stability.

d) The convergence of the present coupled method is good. In addition, the accuracy of the new presented coupled method is slightly worse than that of the pure meshfree method. However, the convergence rates of these two techniques are nearly same.

e) Numerical examples have proven the newly developed coupled method is effective for stress analysis of solids and structures.

In summary, the coupled method allows the advantages of both FEM and meshfree methods to be used. The merits using this coupled method include: 1) the computation cost is lower because the meshfree method, which usually has worse efficiency, is only used in a small region; 2) a good accuracy can be obtained because the meshfree method is used in the region with high stress gradients; 3) the compatibility in the transition region between the FEM domain and meshfree domain can be ensured up to higher order. Hence, the present coupled method provides a potential effective numerical tool for many practical problems.

However, some further researches are required including the application of 3D problems and nonlinear problems. They will be our future research objectives.

Acknowledgement

This work was supported by an ARC Discovery Grant.

Reference

Abraham F, Broughton J, Bernstein N and Kaxiras E (1998), Spanning the continuum to quantum length scales in a dynamic simulation of brittle fracture, Europhys. Lett. 44 (1998) 783–787.

Anderson TL(1991), Fracture Mechanics: Fundamental and Applications (1st Ed.) CRC Press.

Atluri SN and Shen SP (2002), The Meshfree Local Petrov-Galerkin (MLPG) method. Tech Sciemce Press. Encino USA.

Atluri SN and Zhu T (1998), A new meshfree local Petrov-Galerkin (MLPG) approach in computational mechanics. Computational Mechanics, 22, 117-127.

Belytschko T, Lu YY and Gu L (1994), Element-Free Galerkin Methods. International Journal for Numerical Methods in Engineering, 37,229-256.

Belytschko T, and Organ D (1995) Coupled finite element-element–free Galerkin method. Computational Mechanics 17, 186-195.

Brebbia CA, Telles JC and Wrobel LC (1984), Boundary Element Techniques. Springer Verlag, Berlin.

Babuska I and Melenk JM (1997), The Partition of Unity Method, Int. J. Numer. Meth. Engrg., 40, 727–758.

Chessa J, Smolinski P, and Belytschko T (2002), The extended finite element method (XFEM) for solidification problems. International Journal for Numerical Methods in Engineering, 53:1959–1977.

Ching HK and Batra RC (2001), Determination of Crack Tip Fields in Linear Elastostatics by the Meshfree Local Petrov-Galerkin (MLPG)Method. CMES, 2 (2), 273-289

Duarte CA(1996), The hp Cloud Method. PhD dissertation, The University of Texas at Austin, USA.

Duarte CA and Kim DJ (2007), Analysis and applications of a generalized finite element method with global-local enrichment functions. Computer Methods in Applied Mechanics and Engineering, 197(6-8):487–504.

Gingold RA and Moraghan JJ (1977), Smooth particle hydrodynamics: theory and applications to non spherical stars. Monthly Notices of the Royal Astronomical Society, 181, 375-389.

Griebel M and Schweitzer MA (2000), A Particle-Partition of Unity Method for the Solution of Elliptic Parabolic and Hyperbolic PDE, SIAM J. Sci. Comput., 22,853–890.

Gu YT and Liu GR (2001a), A meshfree local Petrov-Galerkin (MLPG) method for free and forced vibration analyses for solids, Computational Mechanics 27 (3), 188-198.

Gu YT and Liu GR (2001b), A local point interpolation method for static and dynamic analysis of thin beams, Computer Methods in Applied Mechanics and Engineering, 190, 5515-5528.

Gu YT and Liu GR(2001c), A coupled element free Galerkin/Boundary element method for stress analysis of two-dimensional solids, Computer Methods in Applied Mechanics and Engineering, 190/34, 4405-4419.

Gu YT and Liu GR(2003), Hybrid boundary point interpolation methods and their coupling with the element free Galerkin method. Engineering Analysis with Boundary Elements, 27(9), 905-917.

Gu YT and Liu GR (2005), Meshfree methods coupled with other methods for solids and structures. Tsinghua Science and Technology. Vol. 10 (1), 8-15.

Gu YT and Zhang LC (2006), A concurrent multiscale method for structures based on the combination of the meshfree method and the molecular dynamics. Multiscale Modeling and Simulation 5 (4): 1128-1155.

Hegen D(1996), Element-free Galerkin methods in combination with finite element approaches. Comput. Methods Appl. Mech. Engrg., 135,143-166.

Krok J and Orkisz J (1989), A unified approach to the FE generalized variational FD method for nonlinear mechanics. Concept and numerical approach, 353-362. Springer-Verlag.

Liew KM, Wu YC, Zou GP and Ng TY (2002). Elasto-plasticity revisited: numerical analysis via reproducing kernel particle method and parametric quadratic programming. Int. J. Numer. Meth. Engng; 55, 669–683.

Liszka T and Orkisz J (1977), Finite difference methods of arbitrary irregular meshes in non-linear problems of applied mechanics. In Proc. 4th Int. Conf. on Structural Mech. In Reactor Tech, San Francisco, USA.

Liu GR (2002), Mesh Free Methods: Moving Beyond the Finite Element Method. CRC press, USA.

Liu GR (2008), A generalized gradient smoothing technique and the smoothed bilinear form for Galerkin formulation of a wide class of computational methods, International Journal of Computational Methods, 5 (2), 199–236.

Liu GR and Gu YT (2000a), Meshfree Local Petrov-Galerkin (MLPG) method in combination with finite element and boundary element approaches. Computational Mechanics, 26(6), 536-546.

Liu GR and Gu YT (2000b), Coupling of element free Galerkin and hybrid boundary element methods using modified variational formulation, Computational Mechanics, 26, 2, 166-173.

Liu GR and Gu YT (2001), A local radial point interpolation method (LR-PIM) for free vibration analyses of 2D solids. Journal of Sound and Vibration, 246(1), 29-46.

Liu GR and Gu YT (2005), An introduction to meshfree methods and their programming. Springer Press, Berlin.

Liu WK, Jun S and Zhang Y (1995), Reproducing kernel particle methods. International Journal for Numerical Methods in Engineering 20, 1081-1106.

Melenk JM and Babuska I (1996), The partition of unity finite element method: Basic theory and applications. Computer Methods in Applied Mechanics and Engineering, 139:289–314.

Schweitzer MA (2003), A Parallel Multilevel Partition of Unity Method for Elliptic Partial Differential Equations, LNCSE, vol. 29, Springer.

Strouboulis T, Babuska I, and Copps K (2000), The design and analysis of the generalized finite element method. Computer Methods in Applied Mechanics and Engineering, 181:43–69.

Timoshenko SP and Goodier JN (1970), Theory of Elasticity, 3rd Edition. McGraw-hill, New York.

Wagner GJ and Liu WK(2003), Coupling of atomic and continuum simulations using a bridging scale decomposition, Journal of Computational Physics, 190, 249–274.

Wang QX, Lam KY, Li Hua and Gu YT (2003). Analysis of microelectromechanical systems (MEMS) by meshless Local Kriging (LoKriging) method. Journal of Chinese Institute of Engineers 27 (4), 573-583.

Xiao SP and Belytschko T(2004), A bridging domain method for coupling continua with molecular dynamics, Computer Methods in Applied Mechanics and Engineering, 193, 1645-1669.

Comput Mech (2009) 44:119–131
DOI 10.1007/s00466-008-0359-y

Zhang GY, Liu GR, Nguyen TT, Song CX, Han X, Zhong ZH and Li GY (2007), The upper bound property for solid mechanics of the linearly conforming radial point interpolation method (LC-RPIM). International Journal of Computational Methods, 4(3), 521-541.

Zienkiewicz OC and Taylor RL (2000), The Finite Element Method. 5th edition, Butterworth Heinemann, Oxford, UK.

Comput Mech (2009) 44:119–131
DOI 10.1007/s00466-008-0359-y

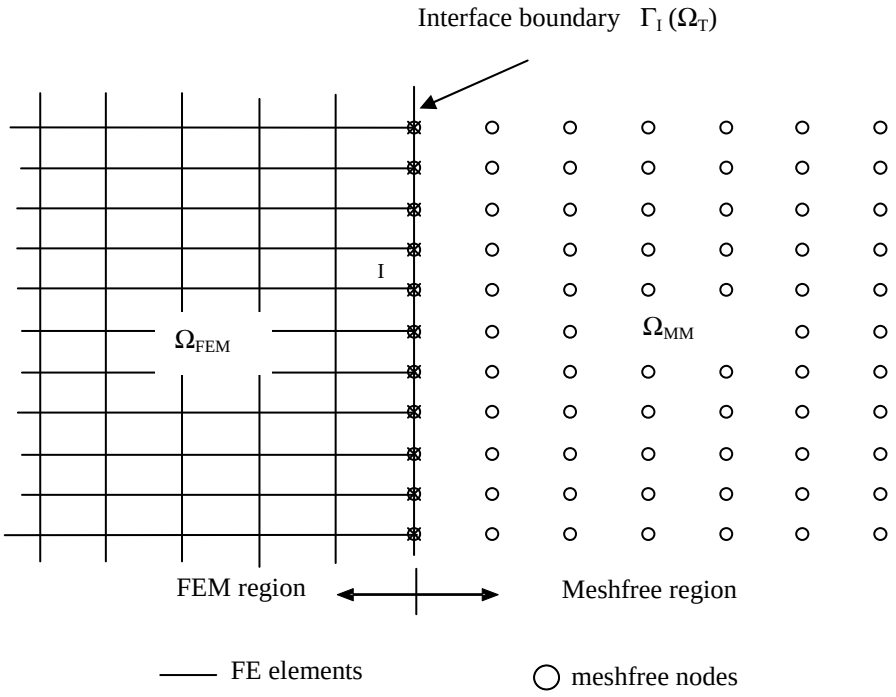

Figure 1 The coupled analysis based on the interface boundary

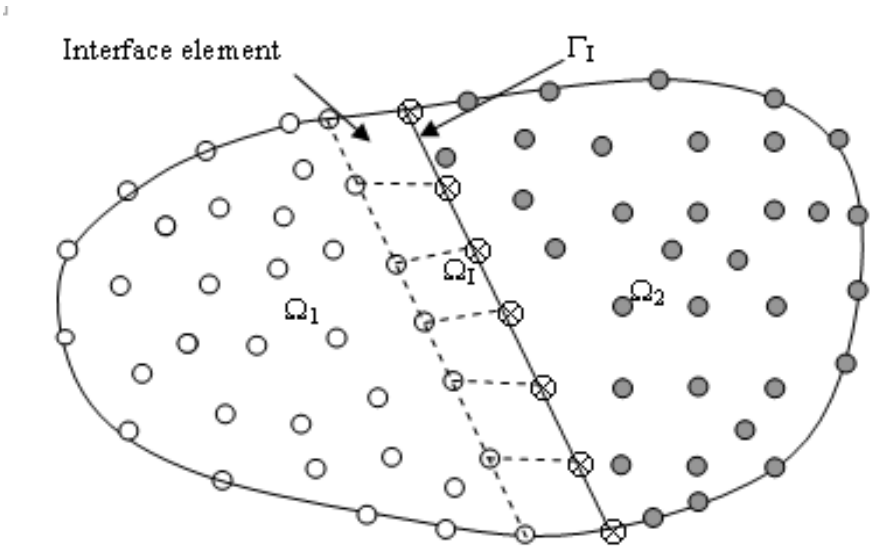

Figure 2 Interface elements used in the coupled method

Comput Mech (2009) 44:119–131
DOI 10.1007/s00466-008-0359-y

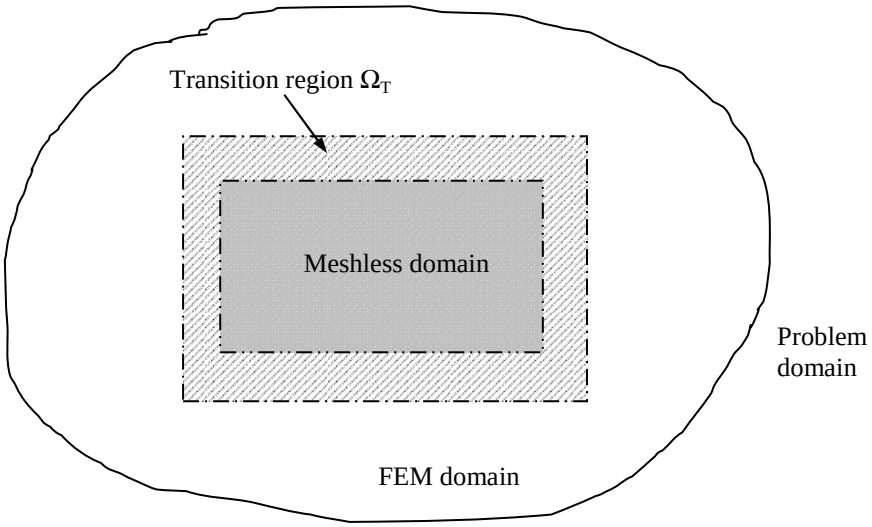

Figure 3 The coupled analysis using the bridging transition technique

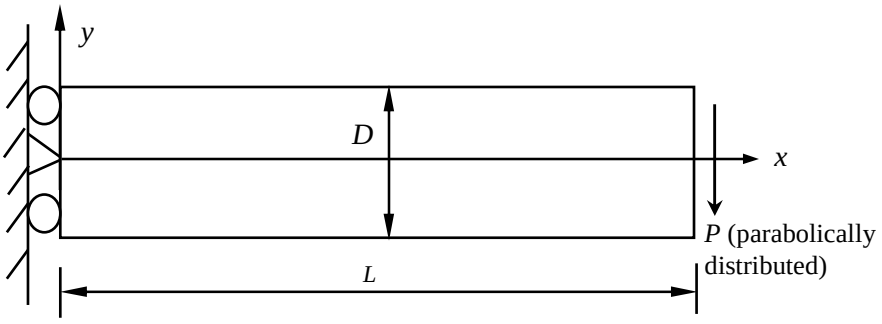

Figure 4 A cantilever beam subjected to a parabolic traction at the free end

Comput Mech (2009) 44:119–131
DOI 10.1007/s00466-008-0359-y

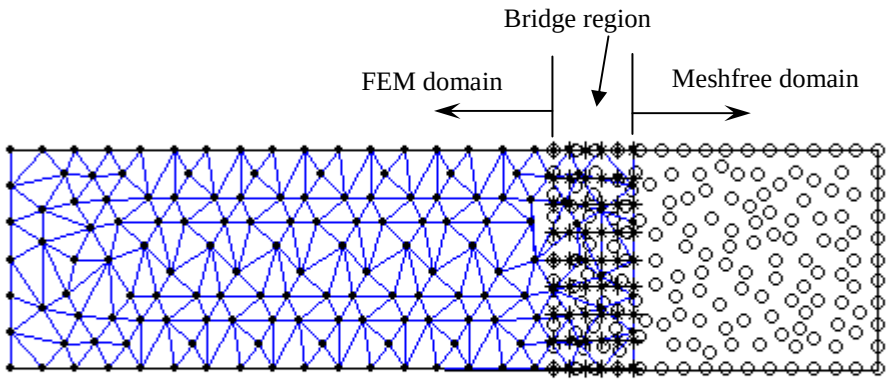

• FEM nodes; o meshless nodes; * transition particles

Figure 5 The computational model for the cantilever beam

Comput Mech (2009) 44:119–131
DOI 10.1007/s00466-008-0359-y

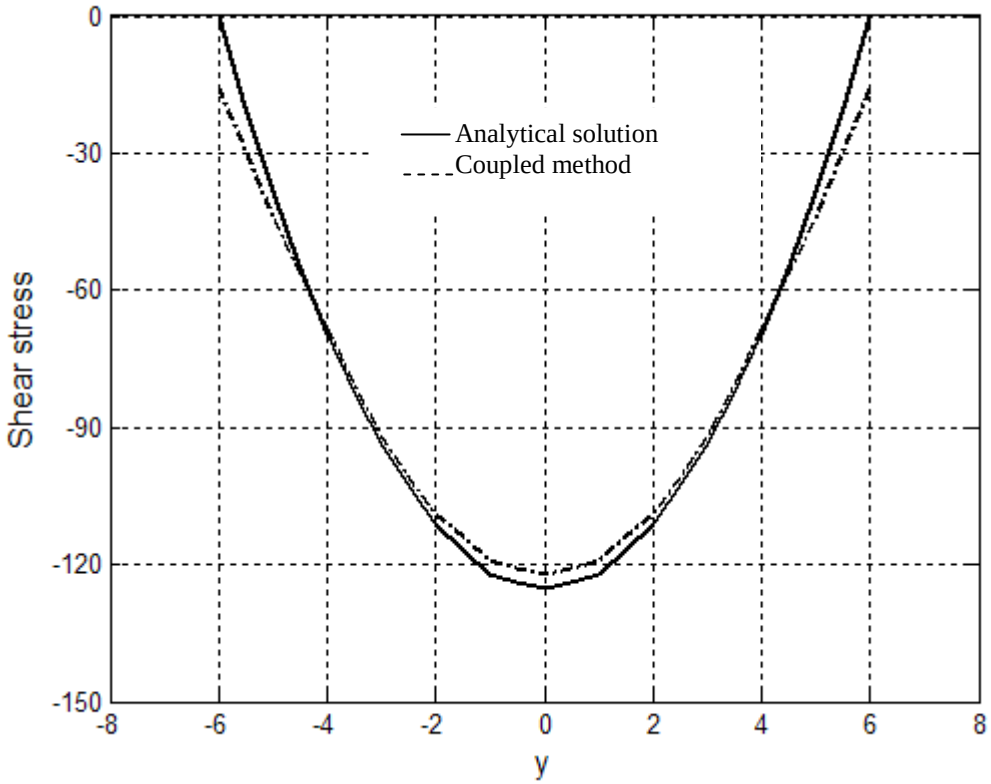

Figure 6 Shear stress on the cross-section at $x=L/2$

Comput Mech (2009) 44:119–131
DOI 10.1007/s00466-008-0359-y

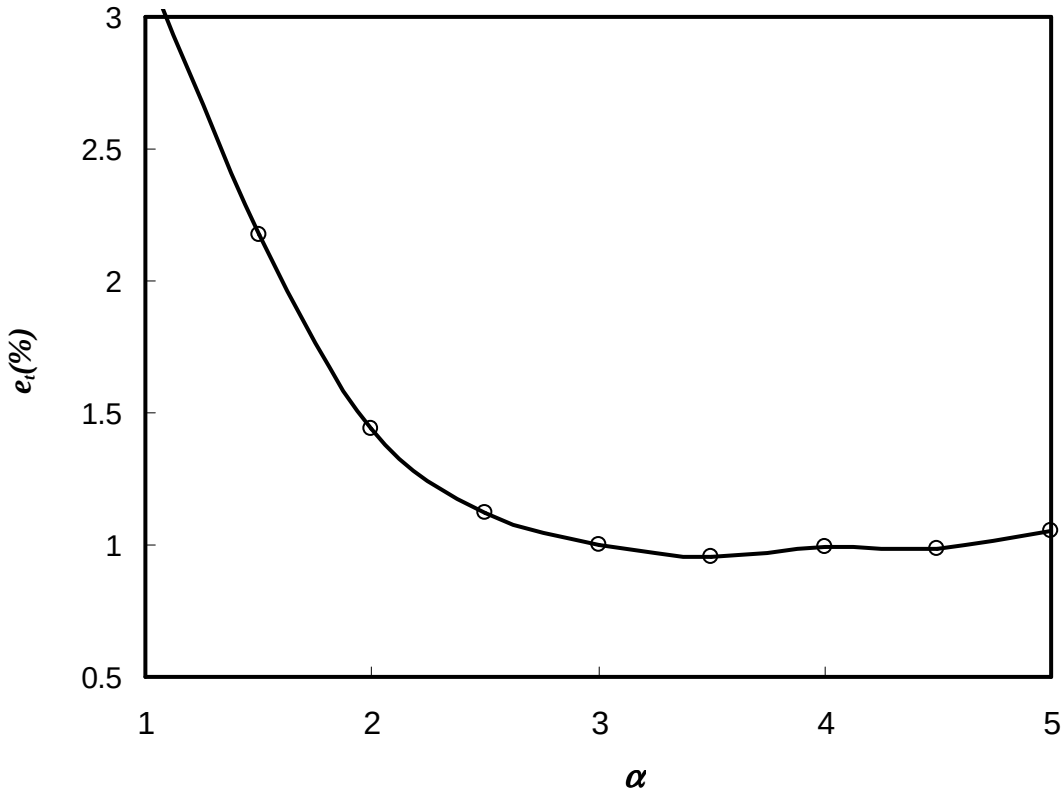

Figure 7 The influence of the size of the transition region

Comput Mech (2009) 44:119–131
DOI 10.1007/s00466-008-0359-y

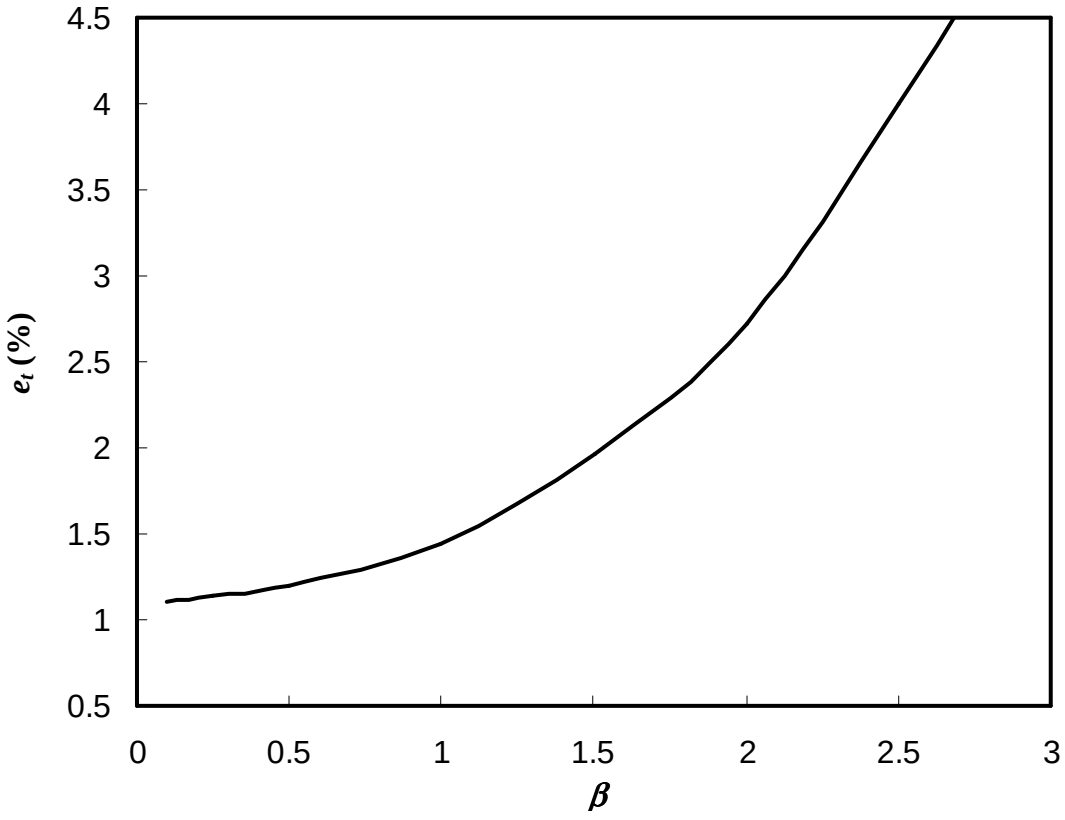

Figure 8 The influence of the distribution of the transition particles

Comput Mech (2009) 44:119–131
DOI 10.1007/s00466-008-0359-y

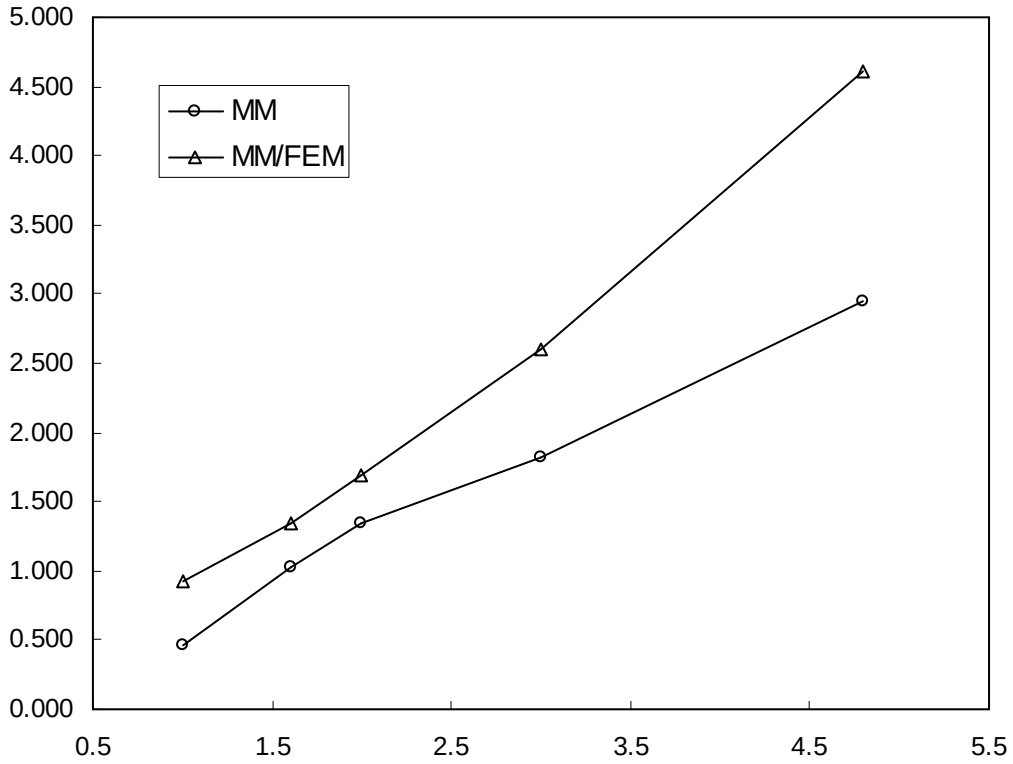

Figure 9 The convergence study

Comput Mech (2009) 44:119–131
DOI 10.1007/s00466-008-0359-y

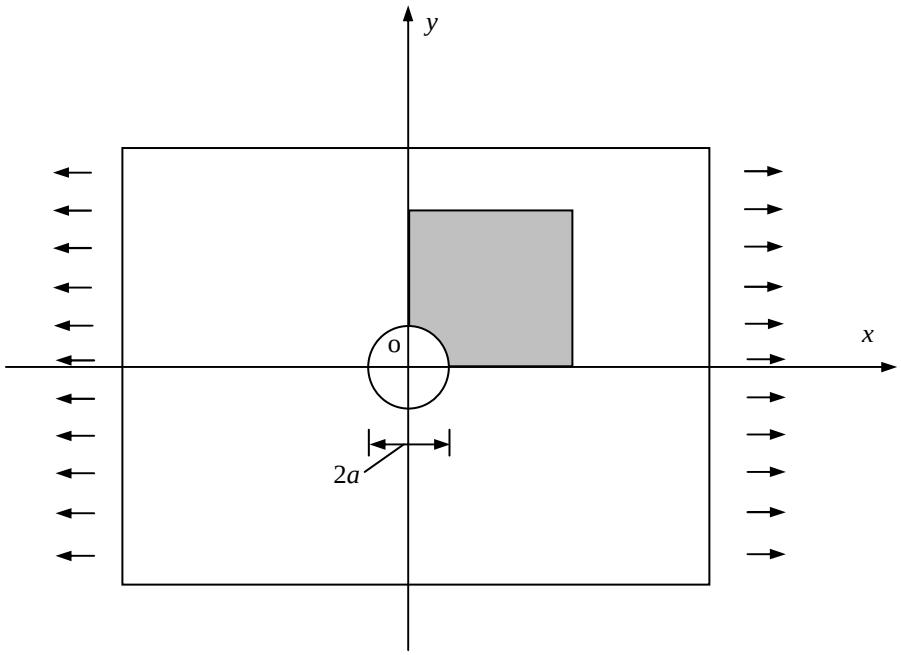

Figure 10 A 2D plate with a central hole subjected to a unidirectional tensile load

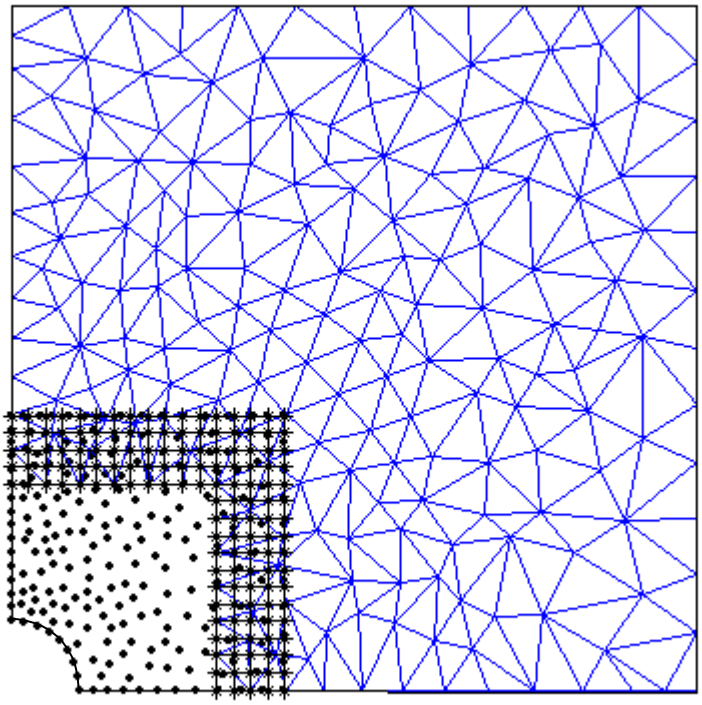

• FEM nodes; o meshless nodes; * transition particles

Figure 11 The computational model for the plate with a hole

Comput Mech (2009) 44:119–131
DOI 10.1007/s00466-008-0359-y

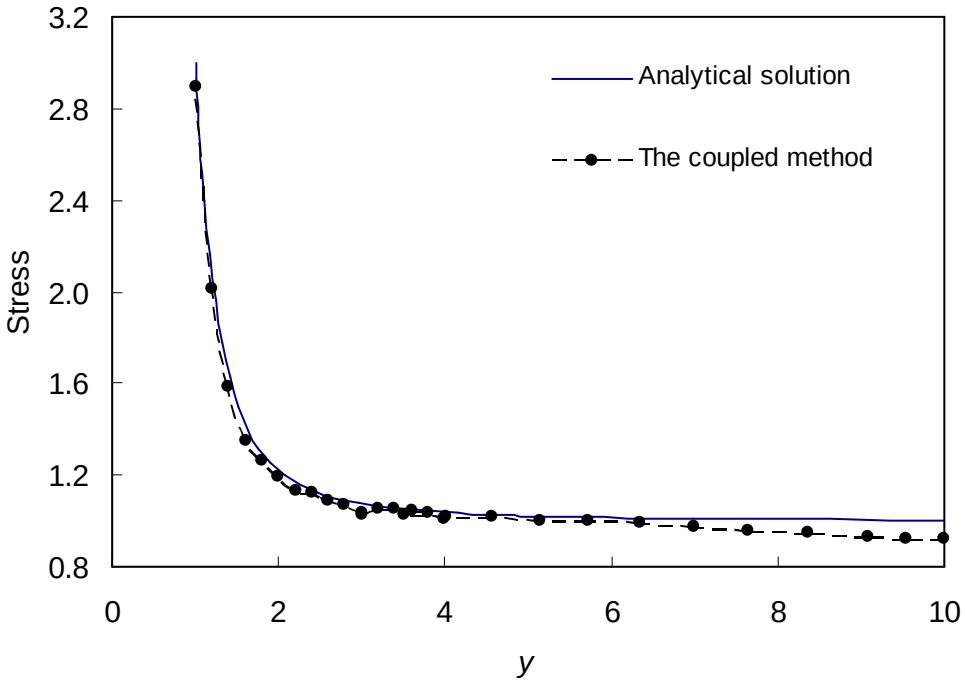

Figure 12 Stress distribution obtained using the coupled method (σ_x, at x=0)

Comput Mech (2009) 44:119–131
DOI 10.1007/s00466-008-0359-y

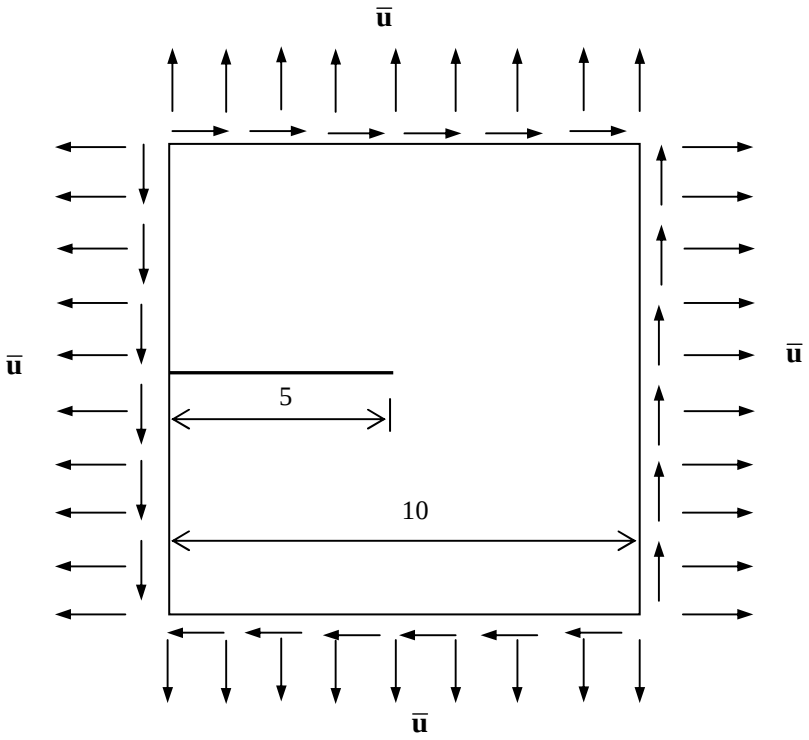

Figure 13 A cracked square plate subjected to Mode-I displacement boundary conditions

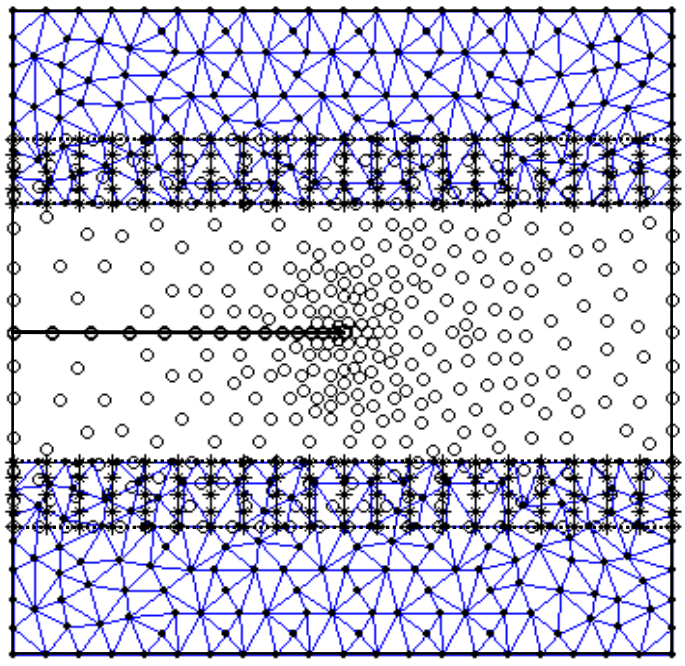

• FEM nodes; o meshless nodes; * transition particles

Figure 14 The computational model for the cracked square plate

Comput Mech (2009) 44:119–131
DOI 10.1007/s00466-008-0359-y

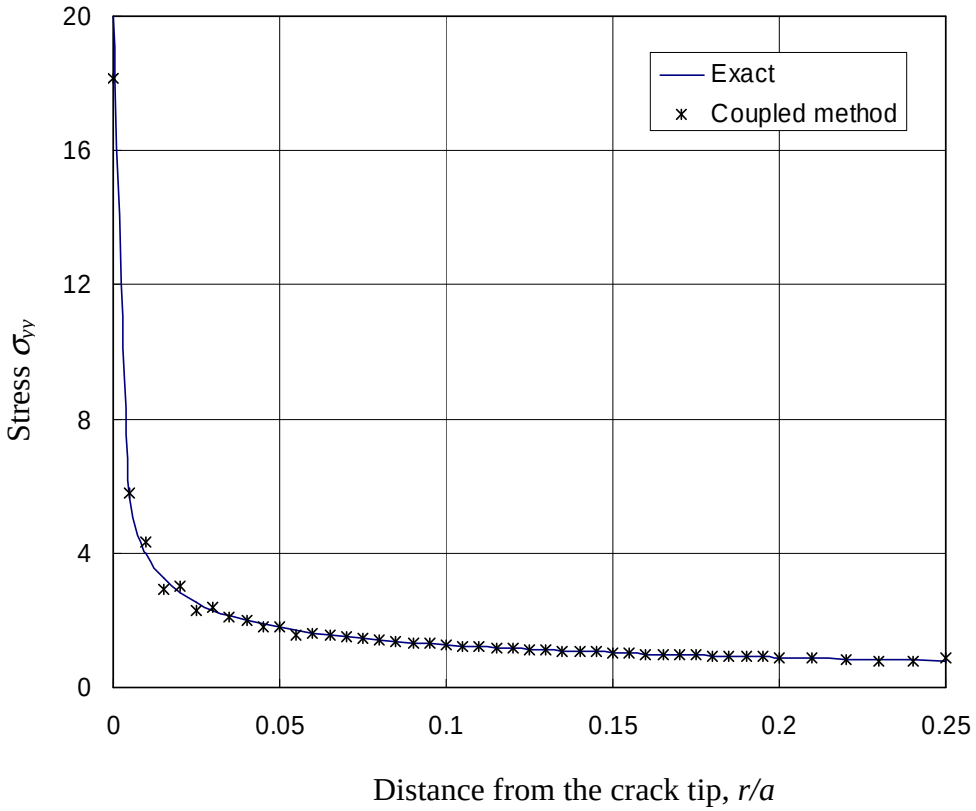

Figure 15 The distribution of σyy along the axis of the crack

Comput Mech (2009) 44:119–131
DOI 10.1007/s00466-008-0359-y

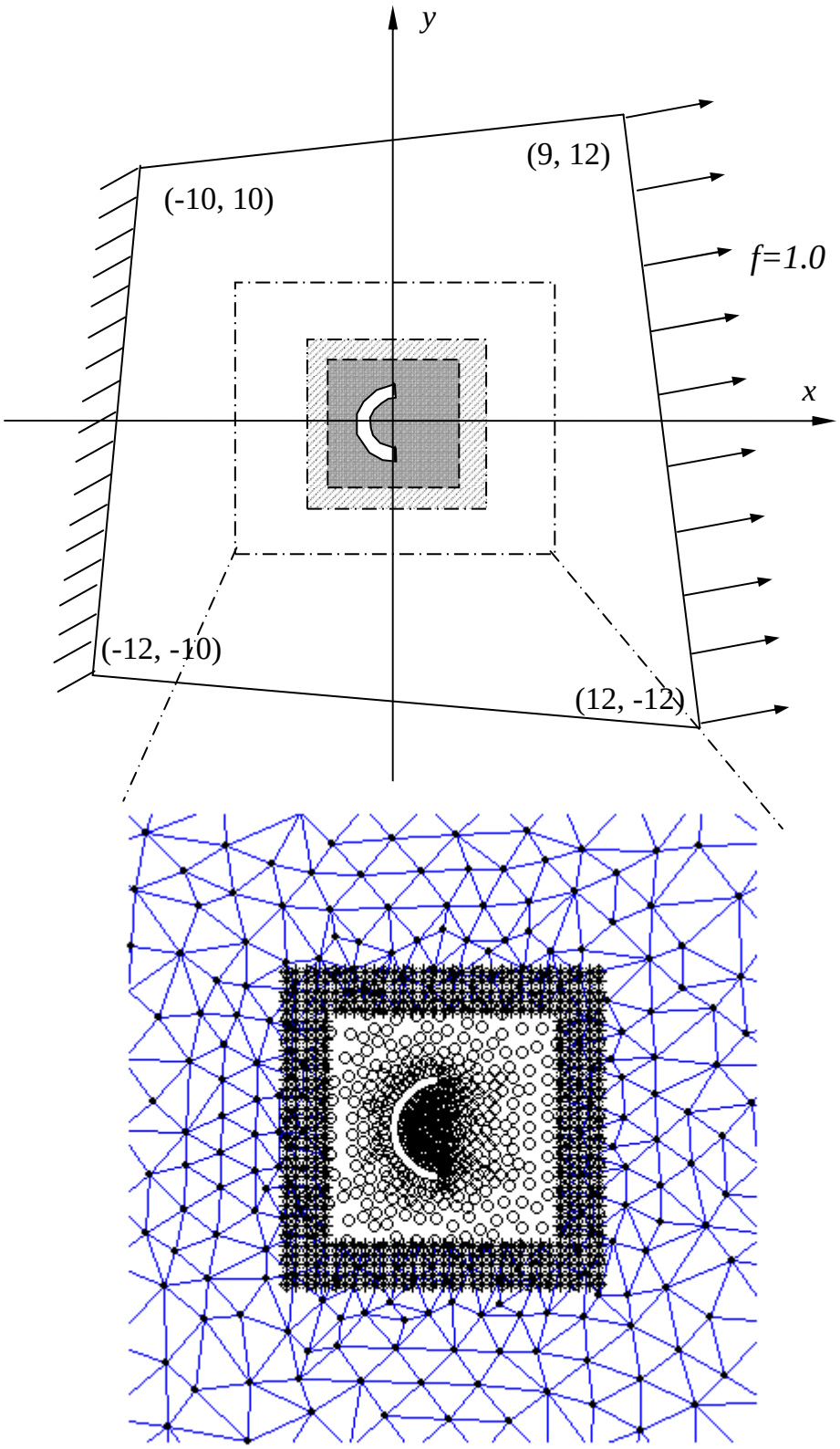

Figure 16 A plate with a complicated hole

Comput Mech (2009) 44:119–131
DOI 10.1007/s00466-008-0359-y

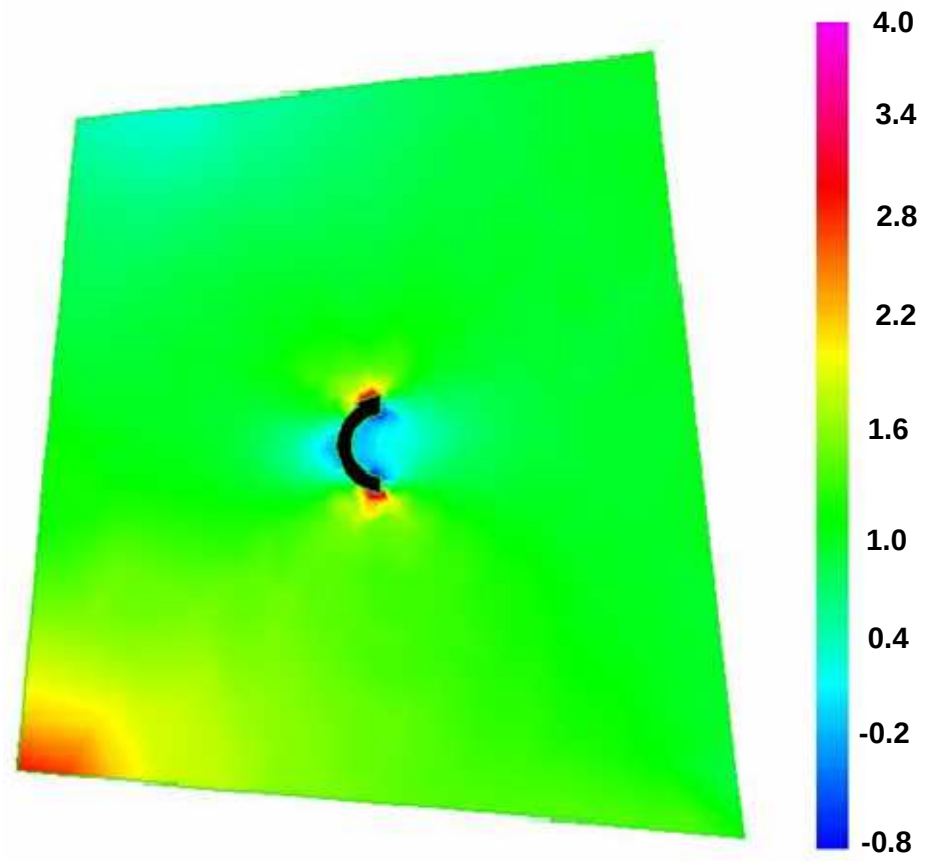

Figure 17 The distribution of σ_{xx}

Comput Mech (2009) 44:119–131
DOI 10.1007/s00466-008-0359-y

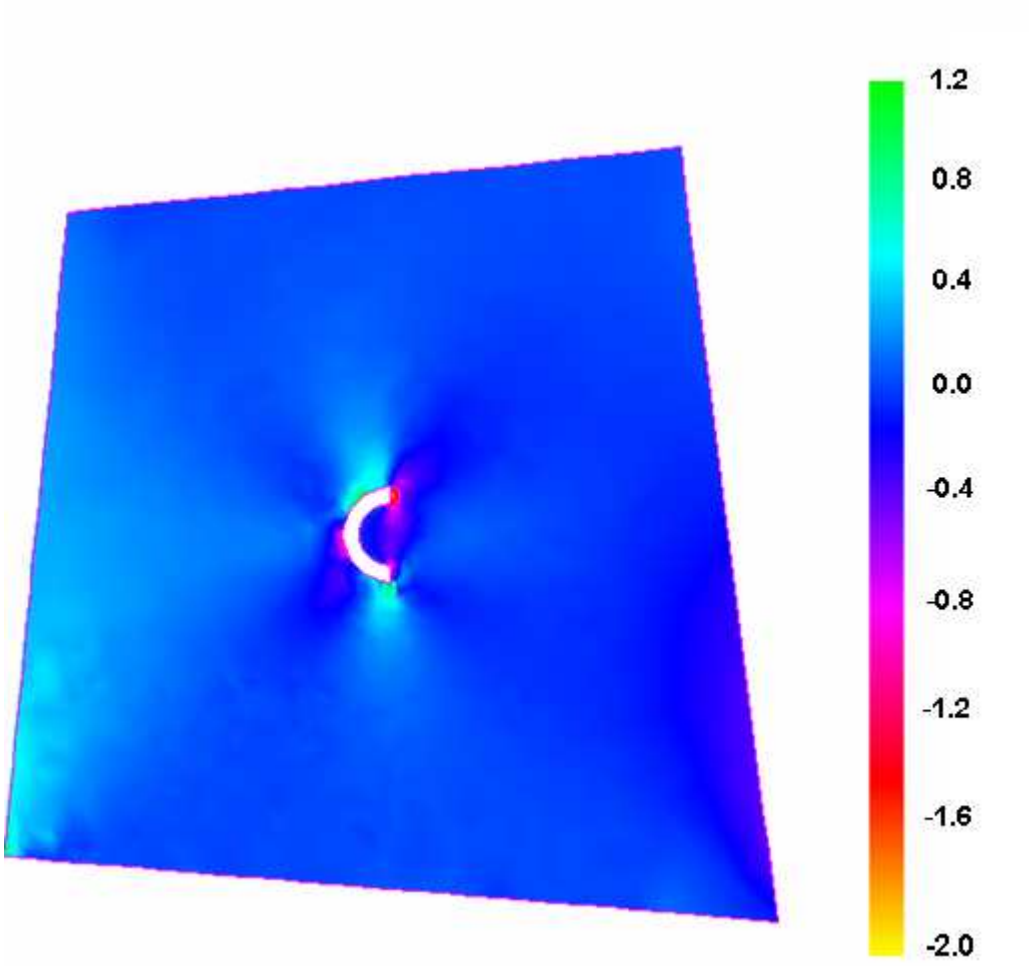

Figure 18 The distribution of σ_{yy}